

Esterase-Responsive Polypeptide Vesicles as Fast-Response and Sustained-Release Nanocompartments for Fibroblast-Exempt Drug Delivery

Weihua Duan, Sifan Ji, Yu Guan, Xueluer Mu, Sha Fang, Yingxi Lu, Xianfeng Zhou,* Jing Sun, and Zhibo Li*



Cite This: <https://dx.doi.org/10.1021/acs.biomac.0c01251>



Read Online

ACCESS |



Metrics & More



Article Recommendations



Supporting Information

ABSTRACT: Enzyme-responsive polypeptide vesicles have attracted considerable attention for precision therapeutics because of their biocompatibility, biodegradability, and unique secondary conformation transition triggered by the catalytic actions of enzymes. These promising potentials of polypeptide vesicles could be limited in a drug delivery system by the very slow enzyme diffusion rate into vesicles that could reduce the efficacy of the drug. On the other hand, stimuli-responsive polymeric vesicles that respond to stimuli can undergo microstructure destruction for the burst release of drugs, which would penetrate through the membrane of dead cells and the tumor extracellular matrix, inducing acute toxicity to neighboring cells. Here, we designed amphiphilic PEG–polypeptide copolymers containing esterase-labile carbamate-caged primary amines. It was found that the diblock can self-assemble into vesicular structures. Esterase-triggered self-immolative decaging reactions could quickly release the primary amine moiety of monomers that can undergo an amidation reaction for transition of the bilayer of vesicles from hydrophobic to partially hydrophilic. This esterase-responsive process retains the nanostructure of vesicles but permeabilizes the vesicle membrane, which can afford the sustained release of encapsulating drugs. These esterase-responsive polypeptide vesicles mediate selective cytotoxicity in cancer cells with high esterase expression over normal fibroblasts with low esterase, enabling the potent anticancer chemotherapy with minimized side effects.



1. INTRODUCTION

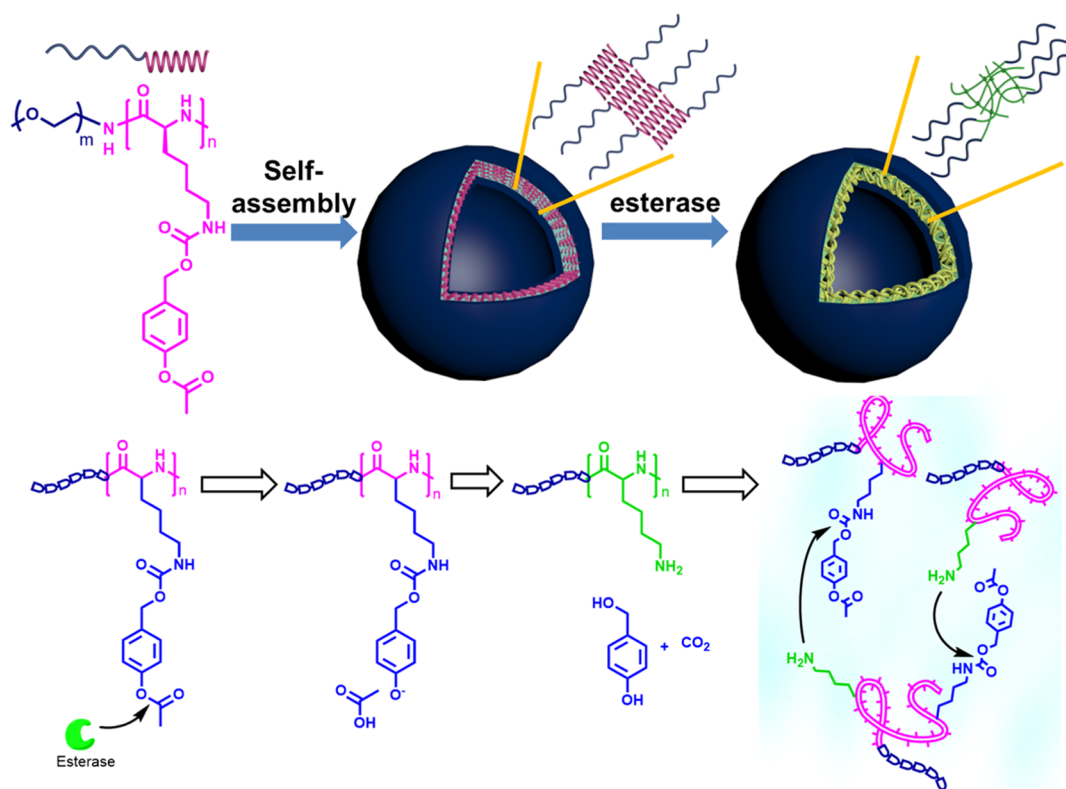
Polypeptide-based nanoassemblies have attracted great research attention in recent years as a result of their prospective application in drug delivery systems because of their biocompatibility and biodegradability.^{1–3} Paclitaxel (NK105)-, doxorubicin (DOX, NK911)-, and cisplatin (NC6004)-loaded polypeptide nanoassemblies have advanced into phase II and phase III clinical trials.⁴ Of all the polypeptide nanoassemblies, nanovesicles are spherical nanostructures that allow the loading and sustained release of both hydrophilic and hydrophobic drugs. The polypeptide vesicles are superior to their lipid counterparts in terms of stability and toughness^{5,6} but could be limited by their very slow release that could reduce the efficacy of the drug. It is important that systemically administered polypeptide vesicles trigger the drug release after they arrive at the target site. Stimuli-responsive polypeptide vesicles have been developed not only to be sensitive to external stimuli such as temperature, light, or ultrasound but also in response to the physiological or pathological variations in the diseased sites such as enzymes, pH, redox, or hypoxia, and so forth.^{7,8} Among them, enzyme-responsive copolypeptide vesicles are particularly attractive because of the high selectivity of enzymatic reactions that can

be conducted under physiological conditions.^{9–15} Particularly, these polypeptides could adopt certain ordered conformations such as α -helices and β -sheets to self-assemble into precious biomimetic structures, which could undergo conformational changes or phase transitions in response to enzymes.^{8,16,17} In comparison with chemical stimuli-responsive polymeric vesicles, the enzyme-responsive polypeptide vesicles have shown a slower response to stimuli with delayed drug release.^{7,18–20} As an enzyme catalyzes a reaction so efficiently, the diffusion of the enzyme into robust polymeric vesicles could be a rate-limiting step for enzyme-triggered drug release systems. In addition, the enzyme could be consumed during the process, which further prevents the free drugs to release rapidly and be sustained at an effective concentration.

Received: August 25, 2020

Revised: October 16, 2020

Scheme 1. Illustration of a Polypeptide Vesicle That Exhibits Intracellular Esterase-Triggered Bilayer Cross-Linking to Accelerate Drug Release without Compromising the Safety^a



^aAmphiphilic PEG-*b*-PLLNA self-assembles into a vesicle with the hydrophobic bilayer containing PLL whose amines are caged with carbamate. The hydrolysis of phenolic acetate by esterase can yield an unstable phenol, which undergoes spontaneous 1,4-benzyl elimination to release primary amine groups. The amidation reaction then occurs to cross-link the membrane of vesicles to retain the nanostructure, which could limit the release of vesicles from apoptotic cells to result in a slow sustained-release of drug with decreased cytotoxicity to the surrounding CAFs.

Over the past decade, cancer-associated fibroblasts (CAFs) in the tumor microenvironment have been reported as key players among stromal cells, owing to their abundance (up to 80% of tumor mass in pancreatic cancer) and their robust cross talk with cancer cells. For example, chemotherapy preferentially targets CAFs because of the cell resistance of cancer cells, and furthermore, stimulates CAFs to release cytokines such as IL-17A, which could create a chemoresistant niche to maintain cancer cells.²¹ In addition, the damaged CAFs can express WNT16B, a signal that promotes cancer cell survival and disease progression.²² It is challenging to precisely distinguish cancer cells from CAFs and effectively eliminate all cancer cells while leaving CAFs unharmed, which would lead to better prognosis. As a representative enzyme, cytosolic esterase presents a high expression level in cancer cells but a low level in fibroblasts,^{23,24} which have been considered as a biomarker for the diagnosis and treatment of cancer. By taking advantage of the altered expression levels, esterase-responsive polymeric vesicles (polymersomes) have been successfully demonstrated for drug delivery applications.^{25–27} Again, the slow and delayed release of drugs from these polymersomes were observed. On the other hand, the exclusive rupture of vesicles could be realized to release almost all the encapsulated drugs once a fast enzyme response is achieved. The released drugs could induce the apoptosis of cancer cells, which would be packaged into small packets of membranes for “garbage collection” (phagocytosis).²⁸ However, the burst-released free drugs induced by vesicle rupture would more readily penetrate

through the membrane of dead or dying cells and the tumor extracellular matrix, which may induce acute toxicity to neighboring cells such as CAFs.²⁹ The contradiction between the fast enzyme response and rupture-induced burst release is a prominent dilemma, and the esterase-responsive polypeptide-based vesicles, for safe and efficient drug delivery, are still very challenging but highly desired.

Recently, chemical cross-linking approaches have been developed to provide the stability of nanostructures and modulate the trafficking of drug molecules, which may address parts of the concerns. Liu and co-workers fabricated the polymersomes containing UV- or H₂O₂-labile carbamate-caged amines, which could exhibit the light- or oxidation-induced “traceless” cross-linking of bilayers with concomitant membrane permeability switching.^{30,31} This strategy may enable the fabrication of enzyme-responsive polypeptide vesicles with balanced stability and permeability. The enzyme-regulated cross-linking of vesicle membranes could simultaneously release drugs but retain the nanostructures, which would induce the apoptosis of tumor cells. Although these exposed vesicles could continue to release its payload like a “Pandora’s box”, the less efficient release of vesicles from apoptotic cells along with the controlled release of drugs would decrease the cytotoxicity to the surrounding CAFs and further optimize the pharmacokinetics. In this study, we constructed a cancer-cell-selective but CAF-exempt polypeptide vesicle for drug delivery using esterase as a trigger. 4-Acetoxybenzyl carbamate, an esterase-responsive moiety was incorporated into the poly-L-

lysine (PLL) side chain using the postmodification method. The obtained PEG-*b*-PLL(*N*-acetoxybenzyl acetate) (PEG-*b*-PLLNA) copolypeptides were expected to undergo self-assembly into nanovesicles in the aqueous solution. Esterase catalyzed the hydrolysis of phenolic acetate moieties, followed by self-immolative decaying reactions to generate the primary amines. Simultaneously, the amidation reactions could occur to cross-link the membrane, which transitioned the membrane from hydrophobic to hydrophilic to accelerate the release of drug from vesicles without compromising the colloidal stability (Scheme 1). The anticancer effects of doxorubicin hydrochloride (DOX)-loaded PEG-*b*-PLLNA vesicles were evaluated *in vitro* and *in vivo*.

2. MATERIALS AND METHODS

2.1. Materials and Apparatus. L-Lysine was bought from GL Biochem (Shanghai) Ltd. α -Methoxy- ω -amino poly(ethylene glycol) (mPEG-NH₂, M_n = 5000 g/mol) was bought from JenKem Technology Co, Ltd (Beijing, China). PEG-*b*-PLL copolypeptides were synthesized by *N*-carboxyanhydride (NCA) ring-opening polymerization (ROP) following the method reported in ref.³² 4-(Hydroxymethyl)phenol and 4-nitrophenyl carbonochloridate were purchased from Energy Chemical. Esterase from porcine liver was from Sigma-Aldrich. Calcein-AM and ethidium homodimer-1 were procured from Invitrogen (Carlsbad, CA). Hexane and THF were purified by first purging with dry nitrogen, followed by passage through columns of activated alumina. DMF, ethyl acetate, and acetonitrile were purchased from Energy Chemical and stored on molecular sieves. All other reagents were bought from commercial suppliers and used without further purification unless otherwise stated.

¹H NMR and ¹³C NMR spectra were recorded on a Bruker AV400 FT-NMR spectrometer. All infrared spectroscopy measurements were performed on a JASCO FT/IR-4700 spectrofluorometer. UV-vis spectra were recorded on a Shimadzu UV-2910 spectrophotometer. Fluorescence spectra were recorded on a HITACHI F-2700 spectrometer. Fluorescence in cells was visualized with a spectral confocal microscope (Nikon C2+). The block copolypeptide was characterized by tandem gel permeation chromatography (GPC) using an SSI pump connected to a Wyatt Optilab DSP differential refractometer detector with DMF containing 0.02 M LiBr as an eluent at a flow rate of 1.0 mL/min at 50 °C. Polystyrene standards were employed for the GPC calibration. All GPC samples were prepared at concentrations of about 6 mg/mL and analyzed using a TSK-gel G4000Hhr column (30 cm × 7.8 mm). Circular dichroism (CD) spectral analysis of copolypeptides was done on an Applied Photophysics Chirascan CD spectrometer. The solution was placed into a quartz cell with a path length of 0.05 cm. Ellipticity ($[\theta]$ in deg·cm²·dmol⁻¹) = (mdeg × mean residue weight)/(path length in mm × concentration of polypeptide in mg·mL⁻¹). The α -helix contents of the polypeptide were calculated using the equation: % α -helix = $(-\theta_{222} + 3000)/39,000$.

2.2. Methods. **2.2.1. Synthesis of 4-(((4-Nitrophenoxy)carbonyloxy)methyl)phenyl Acetate (Compound 4, Scheme S1).** Compound 2: To a mixed solution of 4-hydroxybenzyl alcohol (compound 1, 19.75 g) and trimethylamine (7.7 mL) in THF (250 mL), acetic anhydride (10.9 mL) was added under a N₂ atmosphere over 5 min at 0 °C. The reaction was stirred overnight at room temperature. The solvent was removed by rotary evaporation. The oily product was dissolved in ethyl acetate, washed with brine, and dried with MgSO₄. Purification by flash column chromatography (petroleum ether: ethyl acetate = 2:1) gave 21.0 g (79.0%, yield) of compound 2 as a clear oily liquid. ¹H NMR (400 MHz, CDCl₃): δ (ppm): 7.36 (d, J = 6.8 Hz, 1H), 7.06 (d, J = 6.8 Hz, 1H), 4.65 (d, J = 4 Hz, 2H), 2.30 (s, 3H).

Compound 4: To a solution of 4-(hydroxymethyl)phenyl acetate (compound 2, 7.38 g) and trimethylamine (7.39 mL) in anhydrous acetonitrile (60 mL), 10.74 g of 4-nitrophenyl carbonochloridate

(compound 3) dissolved in 30 mL of anhydrous acetonitrile was added using a constant-pressure funnel. The reaction was monitored by TLC. After the reaction was completed, the solvent was removed under vacuum. The crude product was dissolved in a minimum amount of ethyl acetate, washed three times with ice water, and dried with MgSO₄. The product was obtained by recrystallization with petroleum ether to get a yellow solid with a yield of 10.96 g (74.5%). ¹H NMR (400 MHz, CDCl₃): δ (ppm): 8.28 (d, J = 7.6 Hz, 2H), 7.47 (d, J = 6.8 Hz, 2H), 7.33 (d, J = 7.6 Hz, 2H), 7.13 (d, J = 6.8 Hz, 2H), 5.28 (s, 2H), 2.32 (s, 3H).

2.2.2. Synthesis of PEG-*b*-PLLNA Block Copolypeptides. Postmodification of preformed polypeptides (PEG-*b*-PLL) was used to prepare the PEG-*b*-PLLNA copolypeptides (Scheme S2). To a solution of PEG-*b*-PLL (250 mg) and 4-(((4-nitrophenoxy)carbonyloxy)methyl)phenyl acetate (compound 4, 63 mg) in 15 mL of anhydrous DMF, triethylamine was added and stirred for 2 days. The obtained polypeptide was precipitated with diethyl ether and dried *in vacuo* (250 mg, yield: 52.1%).

2.2.3. PEG-*b*-PLLNA Vesicle Formation and Characterization. To prepare vesicles, 10 mg of copolypeptide was dissolved in 2 mL of THF and stirred for 3 h. An equal volume of deionized water was added at the rate of 1 mL/h using a microinjector. The mixture was stirred at room temperature until most of the THF evaporated. Then, the mixture was placed in a dialysis bag (MWCO = 2000 Da) and dialyzed against deionized water for 24 h. The deionized water was changed every 4 h. The resulting suspension was made up to volume using a volumetric flask for all subsequent physical studies. To determine the critical micelle concentration (cmc) of the amphiphilic diblock copolypeptide, Nile red was used as a fluorescent probe (excitation at 542 nm) according to the reported method.³³

The preparation of the fluorescent dye or DOX-loaded vesicles was done based on the above process except that the dye or DOX was premixed in THF or deionized water. Referring to the method reported in the literature,³⁴ the drug-loading content (DLC) and the drug-loading efficiency (DLE) were determined by UV-vis absorption spectroscopy.

$$\text{DLC (wt \%)} = \frac{\text{mass of loaded drug}}{\text{mass of loaded drug} + \text{mass of polypeptide}} \times 100\%$$

$$\text{DLE (wt \%)} = \frac{\text{mass of loaded drug}}{\text{mass of feeding drug}} \times 100\%$$

The size distribution of nanovesicles was determined by dynamic light scattering (DLS) measurements using a particle size analyzer (90Plus, Brookhaven Instruments Corp., USA) at a fixed angle of 90°. Meanwhile, the size and morphology of copolypeptide nanovesicles were determined by transmission electron microscopy (TEM), which was performed on a JEOL, JSL-2100 operating at 200 kV accelerating voltage.

2.2.4. Esterase-Responsiveness of the Copolypeptide Vesicles. First, the enzymatic responsiveness of copolypeptide vesicles was measured by incubation with porcine liver esterase (10 U/mL) at 37 °C for 8 h. 1 mL of sample was taken from the solution for analysis using a CD spectrometer. The solution was freeze-dried, and the obtained dry powder was diluted in D₂O for ¹H NMR measurements. The esterase-responsiveness of copolypeptides was monitored by the growing peaks (δ : 4.56, 2H; 6.92, 2H; 7.31, 2H), which could be assigned to 4-hydroxybenzyl alcohol, the byproduct of self-immolative decaying reactions.

Enzymatic responsiveness of the polypeptide vesicle was also studied with reference to the method reported in the literature.³⁵ In brief, vesicles containing Nile red were diluted in a PBS solution (pH 7.4) containing 0.05 (wt %) NaN₃, and the final vesicle concentration was adjusted to 200 μ g/mL. Esterase stock solution (150 units/mL) was added to the solution below 37 °C, and the change in fluorescence at 620 nm was observed with time for the polypeptide solution. DLS analyses were performed at 24 h time intervals to monitor the esterase-responsive size variation of vesicles. 4 μ L of

samples was withdrawn from the vesicle solution for TEM sample preparation, followed by analyses.

2.2.5. In Vitro Release Profiles. The *in vitro* release behaviors of DOX from polypeptide vesicles were evaluated with a dialysis method using PBS (pH 7.4) as the release medium. Briefly, 2 mL of the polypeptide formulation (0.2 mg/mL) loaded with DOX was introduced into a dialysis tube (MWCO 2000 Da) with or without 4 μ L of esterase. The mixture was submerged fully into PBS (pH 7.4) at 37 °C under continuous shaking. At predetermined time points, the external buffer solution was removed and replaced with fresh medium. The release of DOX was quantified by measuring the fluorescence with emission at 593 nm (excitation at 480 nm) against a standard curve.

2.2.6. Cell Culture and In Vitro Cytotoxicity Assay. HeLa (human cervical cancer cells) and L929 (mouse fibroblasts) cells were cultured in DMEM supplemented with 10% fetal bovine serum (FBS), 100 U/mL penicillin/streptomycin in an atmosphere of 5% CO₂ and 95% air at 37 °C.

To characterize the interaction between cells and DOX-loaded vesicles, HeLa and L929 cells were cocultured with DOX-loaded vesicles for 4 h. The cells were washed twice with PBS buffer, treated with Hoechst 33342 and LysoTracker Green for 15 min, and then subjected to confocal microscopic analysis.

In vitro cytotoxicity of DOX-loaded vesicles against HeLa and L929 cells was evaluated using both MTT assay and live/dead staining. Briefly, 1 \times 10⁴ cells were seeded in a 96-well plate and maintained in 100 μ L of DMEM supplemented with 10% FBS and 1% antibiotic. After 24 h, the cells were treated with new medium containing different concentrations (3.2, 6.4, 12.8, and 25.6 mg/L DOX equivalent) of free DOX or DOX-loaded polypeptide vesicles for 24 h. The drug-containing medium was discarded and replaced with 100 μ L of serum-free medium. Then, MTT reagent (20 μ L) was added to each well and incubated with cells for another 4 h. The medium was removed and replaced by 100 μ L of DMSO. The absorbance of the solution was measured on a Tecan Infinite 200 PRO microplate reader at 492 nm. Each experimental condition was performed in a quadruple and the data are shown as the mean value plus standard deviation (\pm SD). To further visualize the cell viability, cells treated with free DOX or polypeptide vesicles were stained with the LIVE/DEAD assay kit. Fluorescence imaging of cells was evaluated and recorded using an inverted fluorescence microscope OLYMPUS IX73.

2.2.7. In Vivo Antitumor Efficiency. All animal studies were approved by the Department of Science and Technology of Shandong Province and the Laboratory Animal Center of Qingdao Hao Biological Engineering Co., Ltd. A human cervical cancer cell xenograft tumor model was generated by the subcutaneous injection of HeLa cells (3 \times 10⁶ cells, 100 μ L in PBS) in the left flank of each mouse. When the tumor volume reached \sim 30 mm³, mice were randomly divided into three groups ($n = 5$) and treated with PBS (group 1), free DOX (5 mg/kg, group 2), and DOX-loaded polypeptide vesicles (5 mg/kg DOX, group 3) intravenously *via* the tail vein on days 0, 4, 8, and 12. The tumor volume and body weight were measured every 2 days to evaluate the antitumor activity and systematic toxicity of the vesicles. The tumor volume was calculated based on the equation ($V = (a \times b^2/2)$), where a and b represented the longest and shortest diameter of the tumors, respectively. On day 27, all the mice were sacrificed. Tumors were photographed and then embedded in formalin. 5 μ m thick sections were placed on polylysine-coated slides and stained with hematoxylin and eosin (H&E).

2.2.8. Statistics. Data are represented as mean \pm SD from \geq 3 replicates. Comparisons were made using one-way ANOVA with post hoc testing or Student's t test. Observations were considered to be significantly different for * $p < 0.05$.

3. RESULTS AND DISCUSSION

Phenolic acetate was used as a trigger for designing the esterase-responsive polypeptide because alkyl esters are generally very stable and hydrolyzed very slowly, even in the presence of an enzyme.^{24,36} The PEG-*b*-PLL copolypeptide,

readily obtained *via* ROP of ϵ -benzyloxycarbonyl-L-lysine NCA (Z-Lys NCA) initiated by PEG-NH₂ ($M_n = 5.0$ kg/mol) and deprotection using HBr/HAc, had an M_n close to that of our design (PEG₁₁₃-*b*-PLL₂₀, Table 1). The degree of polymer-

Table 1. Structural Parameters of Esterase-Responsive Block Polypeptides

entry	[M]/[I] ^a	M_n^b (kDa)	M_n^c (kDa)	PDI ^c	GD ^d (%)
PEG ₁₁₃ - <i>b</i> -PLL(Z)	20	10.3	17.9	1.11	
PEG- <i>b</i> -PLL		7.6			
PEG ₁₁₃ - <i>b</i> -PLLNA		11.5	18.4	1.08	\sim 100

^aNumber indicates the monomer/initiator ratio. ^bMolecular weight determined by NMR spectroscopy. ^cMolecular weight and PDI determined by GPC. ^dGD determined by NMR spectroscopy.

ization (DP) of PEG₁₁₃-*b*-PLL₂₀ was determined by comparing the integration of the methylene amine peak (d', $-\text{CH}_2-\text{NH}_2$) with that of the methylene peak of poly(ethylene glycol) (e', $-\text{CH}_2-\text{CH}_2-$). The subscripts present the average DP of PEG and PLL. 4-Acetoxybenzyl carbamate was conjugated to the amine group of PLL to render the polypeptide sensitive to esterase (Scheme S2). The chemical structures of synthesized copolypeptides were confirmed by both ¹H NMR and FTIR spectra (Figure 1). The appearance of new peaks at 6.9, 5.1, and 2.3 ppm corresponded to the protons of the LLNA moiety, suggesting the successful graft of 4-acetoxybenzyl carbamate onto the amine of PEG-*b*-PLL. FTIR spectra also showed characteristic peaks at 1715 and 1456 cm⁻¹, which are attributed to the $\nu_{\text{N}-\text{COO}^-}$ and $\nu_{4\text{-acetoxybenzyl}}$ of PLLNA block. The graft degree (GD) of LLNA units in PEG-*b*-PLLNA was determined to be \sim 20 by comparing the integration of the methyl peak (f, $\text{CH}_3-\text{COO}-$) of the 4-acetoxybenzyl group with that of the methylene peak of poly(ethylene glycol) (e, $-\text{CH}_2-\text{CH}_2-$), which indicated that the amine of PEG₁₁₃-*b*-PLL₂₀ is close to quantitative conversion to LLNA (Table 1). GPC analyses further revealed that PEG₁₁₃-*b*-PLLNA₂₀ had a prescribed molecular weight with a narrow molecular weight distribution [polydispersity index (PDI) = 1.08, Table 1, Figure S3].

The PEG₁₁₃-*b*-PLLNA₂₀ copolypeptide was first dissolved in THF, followed by the addition of an equal volume of water and then dialyzed against water. TEM observation confirmed that the PEG₁₁₃-*b*-PLLNA₂₀ copolypeptide could self-assemble into vesicles (Figure 2a) by the solvent-switch method.³⁷ During this process, THF quickly diffused into the water phase, leading to the aggregation of hydrophobic chains and driving the assembly process. After the removal of THF, DLS analysis was performed to show that the blank vesicle (0.2 mg/mL) had a hydrodynamic radius value of 49.8 ± 20.7 nm (Figure 2b), which is in well agreement with that of the TEM observation (9.8–58.9 nm). The vesicles formed stable suspensions without aggregating or precipitating over time. The cmc of the copolypeptide was measured by fluorescence spectroscopy using lipophilic Nile red as a probe. The cmc value of PEG₁₁₃-*b*-PLLNA₂₀ calculated from the inflection point of fluorescence intensity as a function of the logarithmic concentration of polypeptide was about 20 μ g/mL (Figure 2c). We further investigated the conformation of PEG₁₁₃-*b*-PLLNA₂₀ (0.5 mg/mL) in aqueous solutions using CD spectroscopy (Figure 2d), which displayed a classical α -helical conformation, evidenced by the double negative peaks at \sim 208

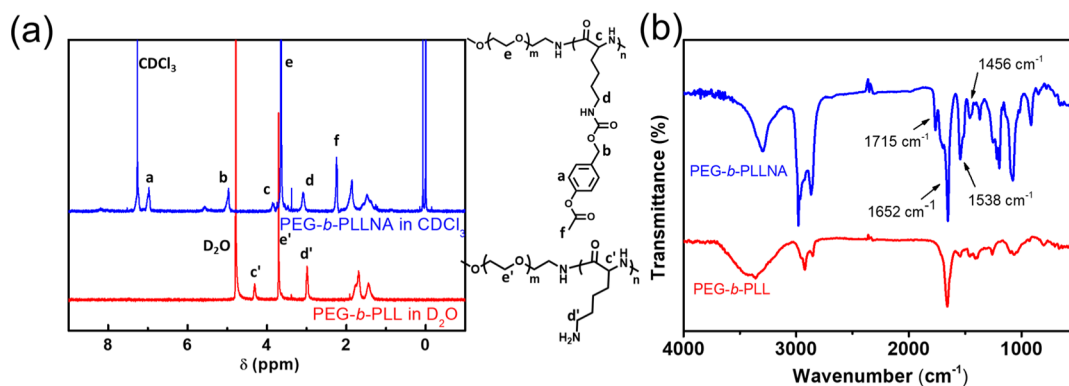


Figure 1. (a) ^1H NMR spectra of PEG-*b*-PLL in D_2O (red line) and PEG-*b*-PLLNA in CDCl_3 (blue line). (b) FT-IR spectra of PEG-*b*-PLL (red line) and PEG-*b*-PLLNA (blue line).

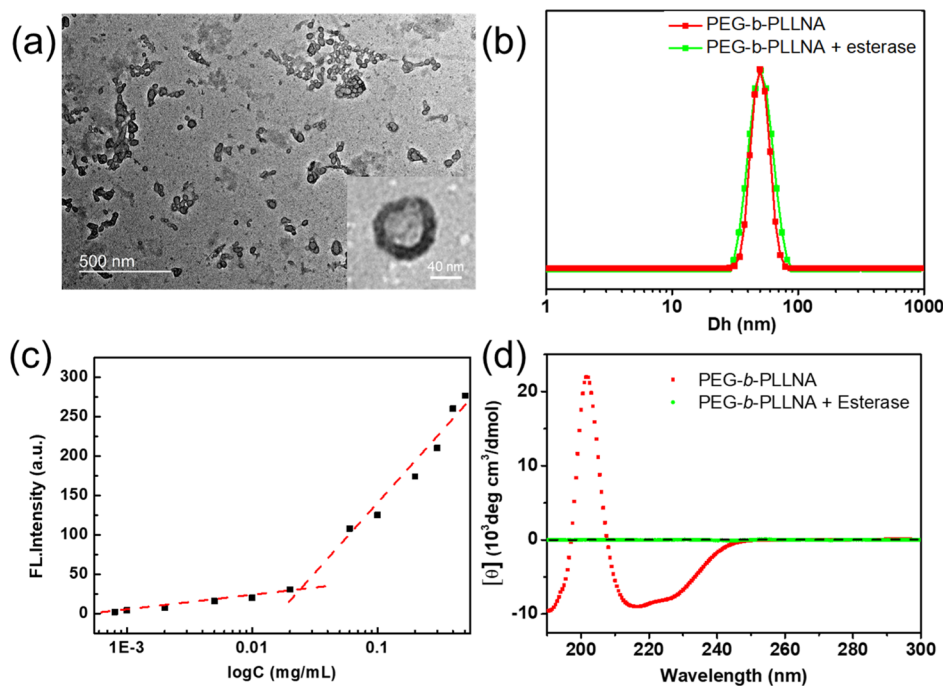


Figure 2. (a) Typical TEM image of PEG-*b*-PLLNA vesicles in an aqueous solution. Scale bar is 500 nm. Inset shows the TEM image of PEG-*b*-PLLNA vesicles treated with 10 U of esterase in aqueous media. Scale bar is 40 nm. (b) Hydrodynamic radius of PEG-*b*-PLLNA vesicles treated with (green) or without (red) esterase (10 U/mL). (c) Critical vesicle concentration of PEG-*b*-PLLNA using Nile red as a fluorescence probe. (d) CD spectra of PEG-*b*-PLLNA vesicles treated with (green) or without (red) esterase (10 U/mL).

and ~ 222 nm. This is consistent with the FTIR spectra (Figure 1b), which exhibited strong absorption at 1652 cm^{-1} (amide I) and 1538 cm^{-1} (amide II) to suggest the helical structure of PEG₁₁₃-*b*-PLLNA₂₀. Therefore, the data indicated that the rod-like PLLNA helices could pack side-by-side along their long axes to form compact vesicles in water (Scheme 1).

We then investigated the esterase-responsiveness of PEG-*b*-PLLNA polypeptide vesicles. Enzyme-catalyzed hydrolysis of phenolic acetate was accomplished by the addition of esterase into the solution of vesicles. In the presence of esterase at 10 U/mL, all the esters were completely hydrolyzed within 8 h. This was confirmed by the complete disappearance of the NMR peaks corresponding to the 4-acetoxybenzyl group of the PLLNA segment and the formation of NMR peaks of 4-hydroxybenzyl alcohol (Figure 3a). This confirmed that esterase triggered the removal of phenolic acetate-capping moieties, followed by self-immolative decaying to generate a primary amine (Scheme 1). It is well known that the secondary

structure of polypeptides can be affected by the side-chain structures.^{38,39} Upon esterase treatment, the initial CD pattern of polypeptide almost disappeared (Figure 2d), indicating a conformational change from helical to disordered. The unwinding of the α -helix was considered to be a prerequisite for the regulation of membrane permeability. DLS studies could provide an insight into the dimensional changes in the hydrodynamic diameters of the nanovesicle upon enzyme treatment. Compared to stimuli-induced dissociation of vesicles, no significant structural (TEM image in Figure 2a inset) and dimensional changes (Figure 2b) were observed for PEG-*b*-PLLNA vesicles after treatment with the enzyme, suggesting the cross-linking of vesicle bilayers. This cross-linking in the nanovesicles could be regarded as the precipitation process in the membrane of the polypeptide, causing a weak signal or no signal on the CD spectra (Figure 2d). Therefore, PEG-*b*-PLLNA polypeptide vesicles exhibited esterase-responsive characteristics, and transformed PLLNA

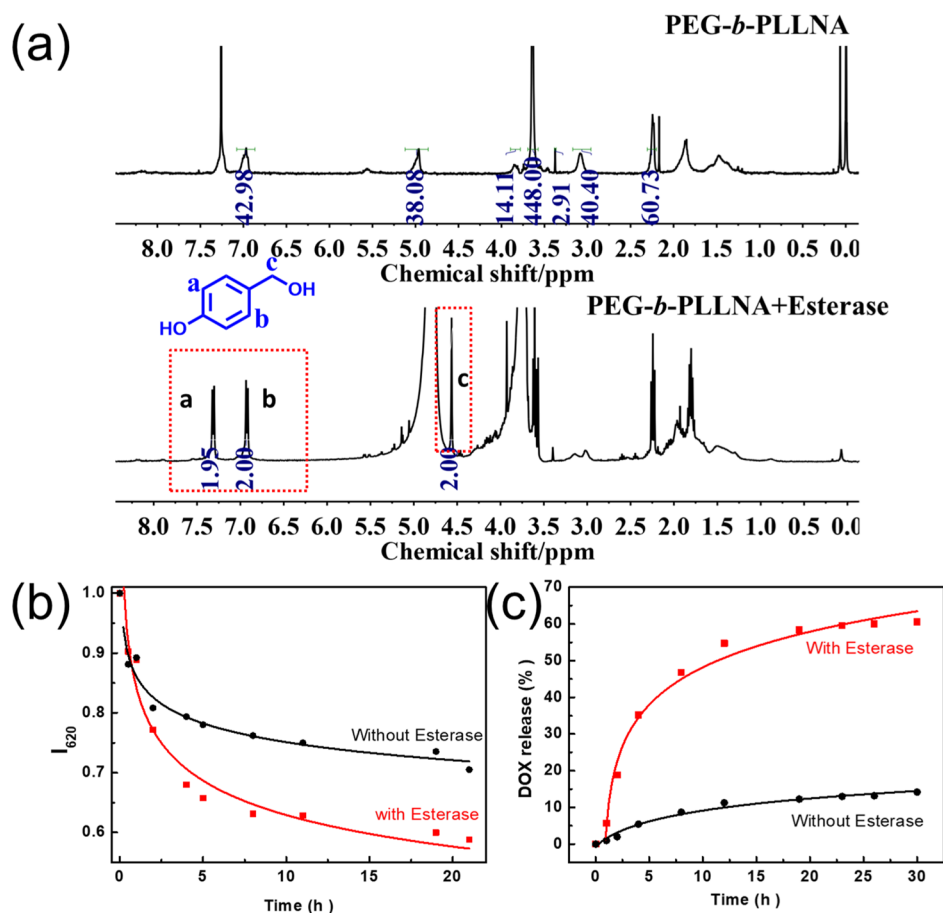


Figure 3. (a) ¹H NMR spectra of PEG-*b*-PLLNA vesicles after treatment with esterase (10 U/mL) for 8 h. (b) Fluorescence intensity (excitation at 542 nm and emission at 620 nm) change of Nile red-loaded PEG-*b*-PLLNA vesicles treated with or without esterase. (c) *In vitro* release of DOX from PEG-*b*-PLLNA vesicles under physiological conditions supplemented with or without esterase.

into PLL, in which the released primary amine simultaneously launched the amidation reactions to retain the vesicle-like structures (Scheme 1).

Polypeptide vesicles are capable of loading and sustained release of both hydrophilic and hydrophobic drugs. Nile red is a solvatochromic dye to display intense fluorescence under a hydrophobic environment but a weak emission in aqueous solutions. In the presence of esterase, the profound loss in fluorescence intensity of Nile red indicates that the polypeptide vesicles underwent a hydrophobic-to-hydrophilic transition (Figure 3b). The accompanied permeability switching of vesicles leads to the immediate release of Nile red, which is mainly caused by the synchronized disappearance of hydrophobic interaction between Nile red and PLLNA block. DOX has hydrophilic regions, which is the first-line drug used for a wide range of cancers. The DLC and DLE of DOX in PEG-*b*-PLLNA vesicles were calculated to be 16.0 ± 1.0 and 49.3 ± 3.5 wt %, respectively. The esterase-triggered release of hydrophilic DOX from the polypeptide vesicles was also studied under physiological conditions. The cumulative release profile of DOX-loaded polypeptide vesicles in the absence or presence of enzyme in PBS (pH 7.4) is shown in Figure 3c, which displayed a biphasic pattern. Initially, in the absence of esterase, only about 5% of DOX was released from vesicles after 4 h of incubation. The slow release of drug is likely to be explained by the stable secondary structure in the vesicle membrane. As a comparison, more than 35% of the drug was

released from the vesicles under enzymatic conditions. This fast enzyme-activated drug release was not anticipated given that the enzyme could not penetrate the hydrophobic membrane to interact with phenolic acetate. A plausible explanation is that esterase first activates the free PEG-*b*-PLLNA, which might diffuse into the membrane of assembled vesicles to initiate the amidation reaction, and then induce the local transition from hydrophobic to hydrophilic. The change in permeability may provide conditions for esterase to penetrate the membrane of the polypeptide vesicle, thereby triggering an enzymatic reaction. The fast enzyme response indicated the accelerated intracellular release inside malignant cells due to the overexpression of esterase, which allowed the free drugs to reach rapidly and be sustained at an effective concentration. Notably, after 12 h, the DOX release from the vesicle was linear over 24 h at a very slow rate. This presented an opportunity for alleviating the acute toxicity issues to the surrounding cells, which could be ascribed to the reserved nanostructure of vesicles without the esterase-triggered vesicle-to-unimer transition. It is thus concluded that PEG-*b*-PLLNA vesicles could facilitate the effective and safe release of DOX into the esterase-overexpressed pathologic environment to show great potency in drug delivery for exerting anticancer effects.

Confocal microscopy was carried out to determine the uptake of polypeptide vesicles into cells. HeLa and L929 cells were costained using the commercially available nuclei-specific

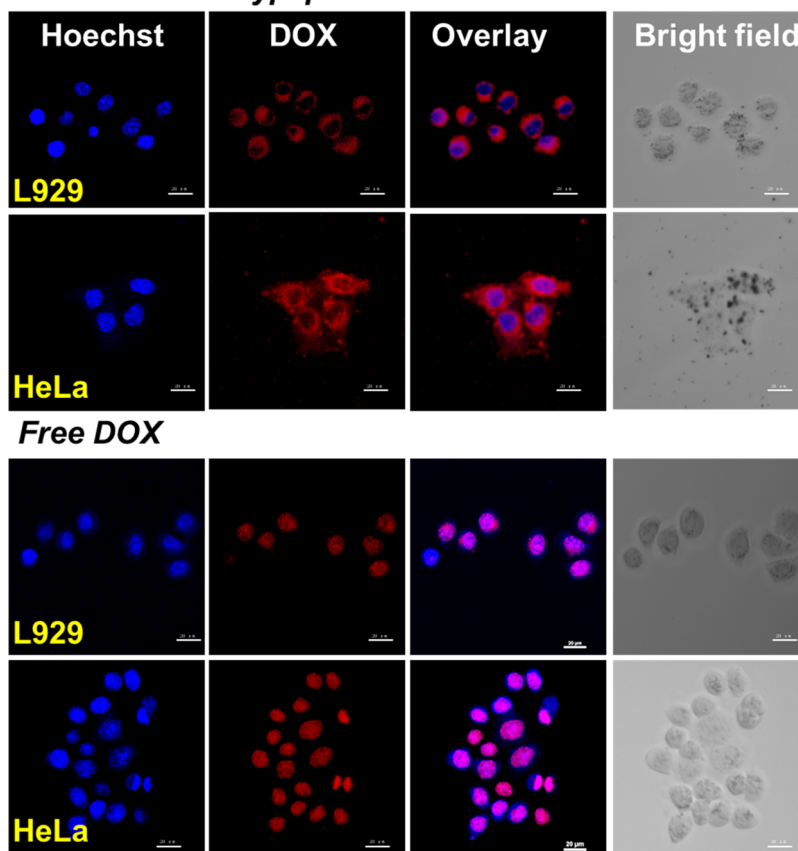
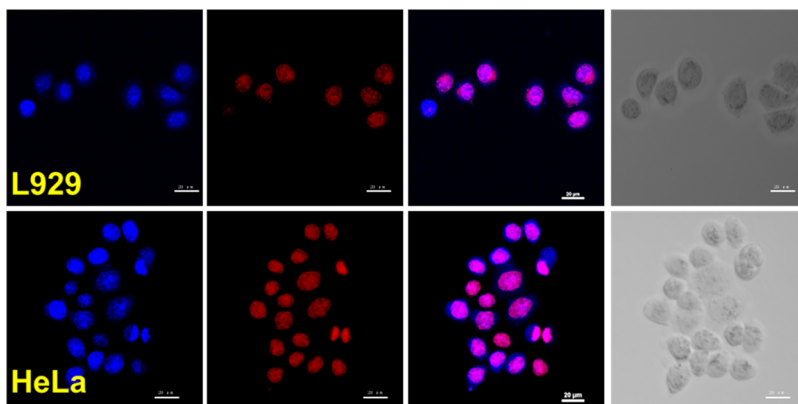
DOX-loaded Polypeptide Vesicles**Free DOX**

Figure 4. Confocal fluorescence images of esterase-responsive DOX-loaded polypeptide vesicles in L929 fibroblasts or HeLa cells. Cell nuclei were stained with Hoechst 33342 shown in blue. Scale bars represent 20 μm.

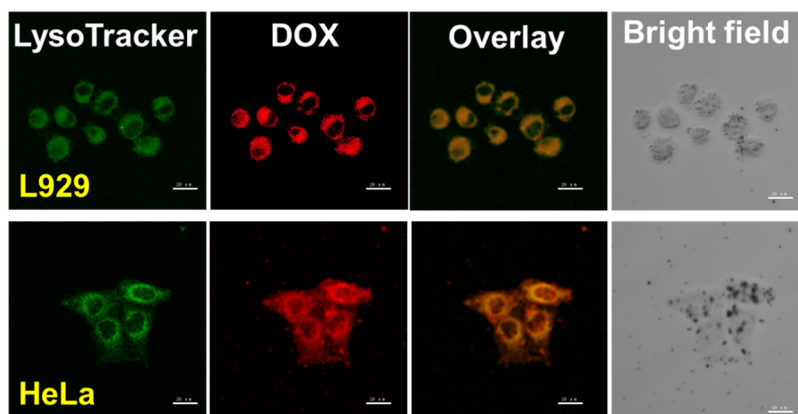


Figure 5. Confocal fluorescence images of esterase-responsive DOX-loaded polypeptide vesicles in L929 fibroblasts or HeLa cells. Lysosomes were stained with LysoTracker shown in green. Scale bars represent 20 μm.

staining probe Hoechst 33342 with the DOX-loaded vesicles (Figure 4). The minimal colocalization of the red emission from DOX-loaded vesicles with the blue emissions from the nuclei-specific Hoechst 33342 showed that the vesicles were mainly distributed in the cytoplasm region, indicating less premature drug release (Figure 4). For comparison, the fluorescence of free DOX and Hoechst 33342 substantially overlapped. To further determine the subcellular distribution of the vesicles, lysosome-specific staining probe LysoTracker Green was used to costain both HeLa and L929 cells with DOX-loaded vesicles (Figure 5). The green fluorescence from

LysoTracker Green is largely correlated with the red fluorescent channel ($R_t = 0.91$ for L929 cells and 0.85 for HeLa cells), which suggests that the majority of the nanovesicles lie inside of the lysosomes. This could be attributed to the clathrin-mediated endocytosis process, which could enhance the interactions with cells to allow the subsequent esterase-triggered DOX release within the cells.

We further evaluated the effect of DOX-loaded PEG-*b*-PLLNA vesicles on the viability of both HeLa cells and L929 fibroblasts using both live/dead staining (Figure 6) and the MTT assay (Figure S4). Free DOX was used as control. The

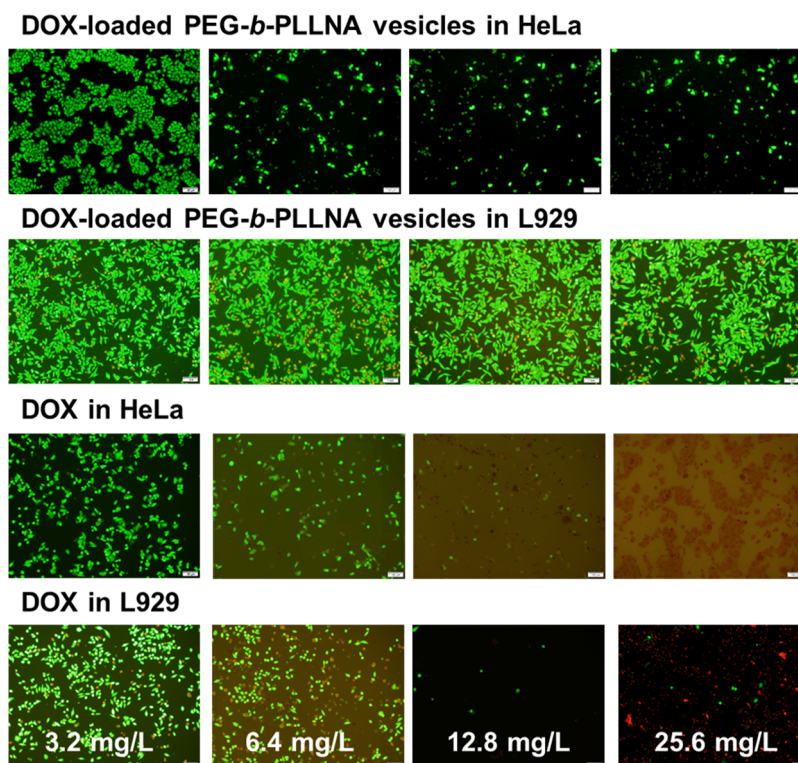


Figure 6. *In vitro* cytotoxicity of DOX-loaded PEG-*b*-PLLNA vesicles evaluated in HeLa and L929 cells at various concentrations using live/dead staining. Viability of free DOX in HeLa and L929 cells was used as control. The concentration of DOX was varied from 3.2 to 25.6 mg/L, corresponding to the respective vesicle concentration from 20.0 to 160.0 mg/L.

concentration of DOX was varied from 3.2 to 25.6 mg/L, corresponding to the respective vesicle concentration from 20.0 to 160.0 mg/L. After 24 h of incubation, free DOX and drug-loaded vesicles showed dose-dependent cytotoxicity. DOX-loaded PEG-*b*-PLLNA vesicles did not exhibit apparent cell killing in L929 fibroblasts at all the tested concentrations. However, the DOX-loaded polypeptide vesicles showed a significant difference in cell killing in HeLa cells, even at lower concentrations (3.2 mg/L). This difference is not caused by the possible different sensitivity of cell to DOX because both cell lines exhibited a similar response to free DOX. HeLa cells showed much higher intracellular esterase activity than L929 fibroblasts,⁴⁰ and the low cytosolic esterase activity in fibroblasts could not efficiently catalyze the hydrolysis of phenolic acetate to trigger the release of cytotoxic DOX from vesicles. Overall, the results of cell uptake and *in vitro* cytotoxicity suggested that the polypeptide vesicle could be effectively taken up and selectively activated by esterase-positive cancer cells to release cytotoxic drugs, thus the esterase-responsive polypeptide vesicles would be a safe and promising drug delivery system.

To further investigate the *in vivo* anticancer efficacy and systematic toxicity of DOX-loaded PEG-*b*-PLLNA vesicles, the BALB/C nude mice bearing HeLa cancer cells were divided into three groups as follows: saline group (PBS), mice treated with free DOX, and mice treated with DOX-loaded polypeptide vesicles (Figure 7a). All the mice were alive during the experimental period. For mice treated with PBS, the tumor continued to grow rapidly, whereas the tumor growth was effectively suppressed in all the groups treated with free DOX or DOX-loaded PEG-*b*-PLLNA vesicles (Figure 7b). Notably, the DOX-loaded vesicles were more effective in

tumor suppression than free DOX in terms of tumor volume ($625.6 \pm 157.7 \text{ mm}^3$ vs $1213.0 \pm 108.1 \text{ mm}^3$, $p < 0.05$) and mass ($730 \pm 20 \text{ mg}$ vs $1100 \pm 27 \text{ mg}$, $p < 0.05$). This effect could be explained by the longer circulation time of PEG-coated formulation, the intracellular accumulation of drugs at tumor sites *via* the enhanced permeability and retention effect, and the esterase-responsive fast release of DOX.^{27,37,41} The histologic analysis of excised tumors from each group also reached a similar conclusion that treatment with DOX-loaded PEG-*b*-PLLNA vesicles resulted in blurred cell morphology and showed dark chromatin with reduced cell densities (Figure 7d), indicating the cancer cell remission. In addition to their therapeutic advantages, DOX-loaded polypeptide vesicles did not show any noticeable toxicity or side effects such as change in the body weights of mice (Figure 7c). It could be explained by the fact that DOX released from vesicles in a sustained manner did not surpass the therapeutic safe level. For comparison, potential acute toxicity was observed for mice treated with free DOX, with a weight loss of approximately ~20% during the treatment stage. These results indicated that PEG-*b*-PLLNA polypeptide vesicles are highly promising for cancer therapy because of their improved therapeutic effects with good biosafety.

4. CONCLUSIONS

In summary, an esterase-responsive polypeptide vesicle was engineered with an enzyme-regulated cross-linking strategy that allowed the sustained and controlled release of drugs with a fast enzyme-activated rate, which could selectively kill cancer cells with high cytosolic esterase expression but conserved fibroblasts owing to their low esterase activity. This unique nanovesicle as a novel drug delivery platform substantially

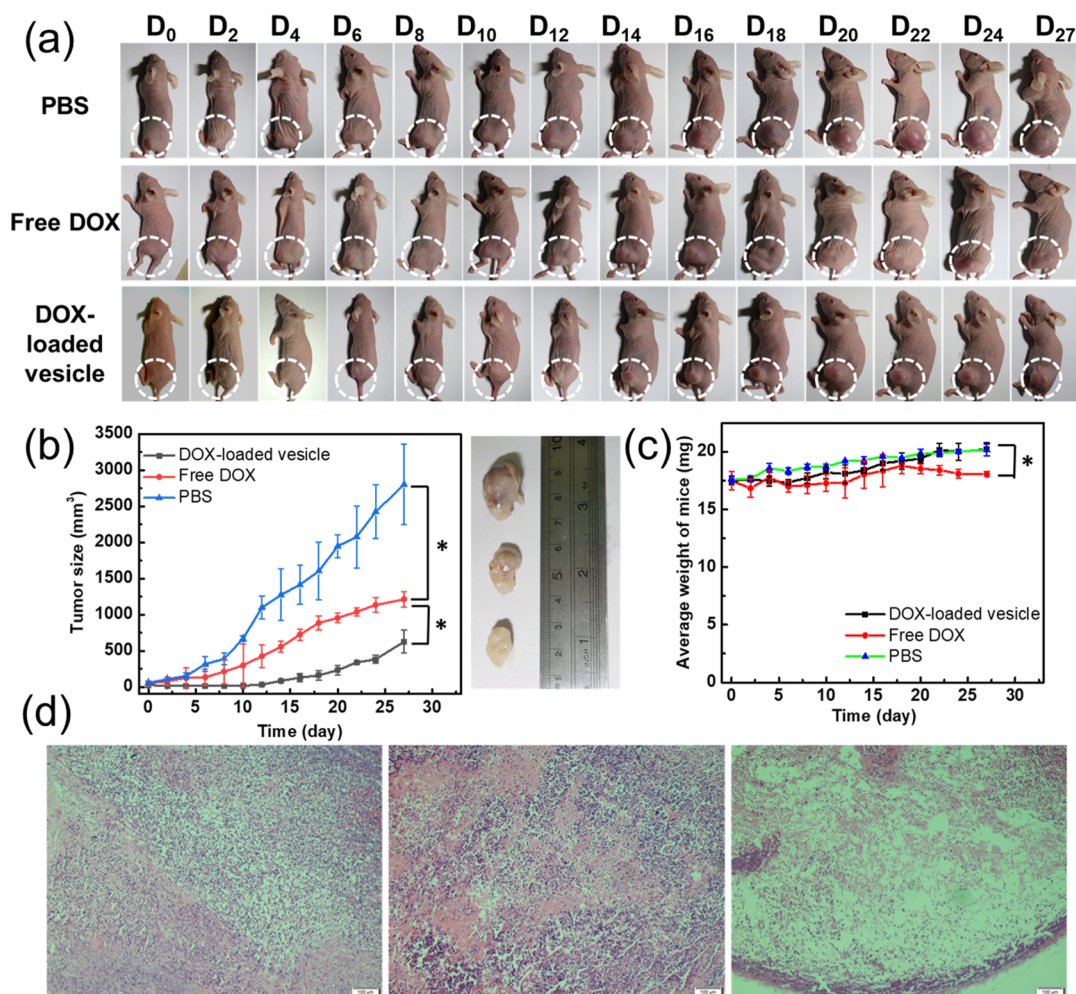


Figure 7. (a) Representative photographs of BALB/c human cervical tumor-bearing mice treated with PBS, free DOX, or DOX-loaded polypeptide vesicles for 27 days. Tumors are indicated by ellipses. (b) Tumor volume and (c) body weight of mice in different groups ($n = 5$). * $p < 0.05$. (d) Representative optical images of *ex vivo* tumor sections assayed by H&E staining.

enhanced the *in vivo* antitumor efficacy but decreased the systematic toxicity to normal cells compared to free DOX at equal doses. These results suggest that this enzyme-responsive polypeptide vesicle can be a promising, safe, and efficient drug delivery system in cancer chemotherapy.

■ ASSOCIATED CONTENT

SI Supporting Information

The Supporting Information is available free of charge at <https://pubs.acs.org/doi/10.1021/acs.biomac.0c01251>.

Synthetic route for PEG-*b*-PLLNA copolypeptides, ^1H NMR spectra of intermediate products, and *in vitro* cytotoxicity of the polypeptide vesicle using the MTT assay (PDF)

■ AUTHOR INFORMATION

Corresponding Authors

Xianfeng Zhou – Key Lab of Biobased Polymer Materials of Shandong Provincial Education Department, College of Polymer Science and Engineering, Qingdao University of Science and Technology, Qingdao 266042, P. R. China; orcid.org/0000-0002-1408-3180; Email: xianfeng@uakron.edu

Zhibo Li – Key Lab of Biobased Polymer Materials of Shandong Provincial Education Department, College of Polymer Science and Engineering and College of Chemical Engineering, Qingdao University of Science and Technology, Qingdao 266042, P. R. China; orcid.org/0000-0001-9512-1507; Phone: +86-532-84022950; Email: zbli@qust.edu.cn

Authors

Weihua Duan – Key Lab of Biobased Polymer Materials of Shandong Provincial Education Department, College of Polymer Science and Engineering, Qingdao University of Science and Technology, Qingdao 266042, P. R. China
Sifan Ji – Key Lab of Biobased Polymer Materials of Shandong Provincial Education Department, College of Polymer Science and Engineering, Qingdao University of Science and Technology, Qingdao 266042, P. R. China
Yu Guan – Key Lab of Biobased Polymer Materials of Shandong Provincial Education Department, College of Polymer Science and Engineering, Qingdao University of Science and Technology, Qingdao 266042, P. R. China
Xueluer Mu – Key Lab of Biobased Polymer Materials of Shandong Provincial Education Department, College of Polymer Science and Engineering, Qingdao University of Science and Technology, Qingdao 266042, P. R. China

Sha Fang – Key Lab of Biobased Polymer Materials of Shandong Provincial Education Department, College of Polymer Science and Engineering, Qingdao University of Science and Technology, Qingdao 266042, P. R. China
Yingxi Lu – College of Material Science and Engineering, Qingdao University of Science and Technology, Qingdao 266042, P. R. China; orcid.org/0000-0002-6046-0362
Jing Sun – Key Lab of Biobased Polymer Materials of Shandong Provincial Education Department, College of Polymer Science and Engineering, Qingdao University of Science and Technology, Qingdao 266042, P. R. China; orcid.org/0000-0003-1267-0215

Complete contact information is available at:
<https://pubs.acs.org/10.1021/acs.biomac.0c01251>

Notes

The authors declare no competing financial interest.

ACKNOWLEDGMENTS

Financial support was provided by National Natural Science Foundation of China (51773107, 51690152, 21704051, and 22071128) and the Taishan Scholars Project of Shandong Province (tsqn201812072).

REFERENCES

- (1) Shen, Y.; Fu, X.; Fu, W.; Li, Z. Biodegradable stimuli-responsive polypeptide materials prepared by ring opening polymerization. *Chem. Soc. Rev.* **2015**, *44*, 612–622.
- (2) Huang, J.; Heise, A. Stimuli responsive synthetic polypeptides derived from N-carboxyanhydride (NCA) polymerisation. *Chem. Soc. Rev.* **2013**, *42*, 7373–7390.
- (3) Bellomo, E. G.; Wyrsta, M. D.; Pakstis, L.; Pochan, D. J.; Deming, T. J. Stimuli-responsive polypeptide vesicles by conformation-specific assembly. *Nat. Mater.* **2004**, *3*, 244–248.
- (4) Cabral, H.; Kataoka, K. Progress of drug-loaded polymeric micelles into clinical studies. *J. Controlled Release* **2014**, *190*, 465–476.
- (5) Thambi, T.; Lee, D. S. 15—Stimuli-responsive polymersomes for cancer therapy. In *Stimuli Responsive Polymeric Nanocarriers for Drug Delivery Applications*; Makhoul, A. S. H., Abu-Thabit, N. Y., Eds.; Woodhead Publishing, 2019; pp 413–438.
- (6) Discher, B. M.; Won, Y.-Y.; Ege, D. S.; Lee, J. C.-M.; Bates, F. S.; Discher, D. E.; Hammer, D. A. Polymersomes: Tough Vesicles Made from Diblock Copolymers. *Science* **1999**, *284*, 1143–1146.
- (7) Liarou, E.; Varlas, S.; Skoulas, D.; Tsimblouli, C.; Sereti, E.; Dimas, K.; Iatrou, H. Smart polymersomes and hydrogels from polypeptide-based polymer systems through α -amino acid N-carboxyanhydride ring-opening polymerization. From chemistry to biomedical applications. *Prog. Polym. Sci.* **2018**, *83*, 28–78.
- (8) Zhou, X.; Li, Z. Advances and Biomedical Applications of Polypeptide Hydrogels Derived from α -Amino Acid N-Carboxyanhydride (NCA) Polymerizations. *Adv. Healthcare Mater.* **2018**, *15*, 1800020.
- (9) Zhang, C.; Pan, D.; Li, J.; Hu, J.; Bains, A.; Guys, N.; Zhu, H.; Li, X.; Luo, K.; Gong, Q.; Gu, Z. Enzyme-responsive peptide dendrimer-gemcitabine conjugate as a controlled-release drug delivery vehicle with enhanced antitumor efficacy. *Acta Biomater.* **2017**, *55*, 153–162.
- (10) Nishimura, T.; Yamada, A.; Umezaki, K.; Sawada, S.-i.; Mukai, S.-a.; Sasaki, Y.; Akiyoshi, K. Self-Assembled Polypeptide Nanogels with Enzymatically Transformable Surface as a Small Interfering RNA Delivery Platform. *Biomacromolecules* **2017**, *18*, 3913–3923.
- (11) Mizukami, S.; Kashibe, M.; Matsumoto, K.; Hori, Y.; Kikuchi, K. Enzyme-triggered compound release using functionalized antimicrobial peptide derivatives. *Chem. Sci.* **2017**, *8*, 3047–3053.
- (12) Nguyen, M. M.; Carlini, A. S.; Chien, M.-P.; Sonnenberg, S.; Luo, C.; Braden, R. L.; Osborn, K. G.; Li, Y.; Gianneschi, N. C.; Christman, K. L. Enzyme-Responsive Nanoparticles for Targeted Accumulation and Prolonged Retention in Heart Tissue after Myocardial Infarction. *Adv. Mater.* **2015**, *27*, 5547–5552.
- (13) Zhang, C.; Pan, D.; Luo, K.; She, W.; Guo, C.; Yang, Y.; Gu, Z. Peptide Dendrimer-Doxorubicin Conjugate-Based Nanoparticles as an Enzyme-Responsive Drug Delivery System for Cancer Therapy. *Adv. Healthcare Mater.* **2014**, *3*, 1299–1308.
- (14) Rodriguez, A. R.; Kramer, J. R.; Deming, T. J. Enzyme-Triggered Cargo Release from Methionine Sulfoxide Containing Copolypeptide Vesicles. *Biomacromolecules* **2013**, *14*, 3610–3614.
- (15) Habraken, G. J. M.; Peeters, M.; Thornton, P. D.; Koning, C. E.; Heise, A. Selective Enzymatic Degradation of Self-Assembled Particles from Amphiphilic Block Copolymers Obtained by the Combination of N-Carboxyanhydride and Nitroxide-Mediated Polymerization. *Biomacromolecules* **2011**, *12*, 3761–3769.
- (16) Fan, J.; Li, R.; Wang, H.; He, X.; Nguyen, T. P.; Letteri, R. A.; Zou, J.; Wooley, K. L. Multi-responsive polypeptide hydrogels derived from N-carboxyanhydride terpolymerizations for delivery of non-steroidal anti-inflammatory drugs. *Org. Biomol. Chem.* **2017**, *15*, 5145–5154.
- (17) Sun, Y.; Hou, Y.; Zhou, X.; Yuan, J.; Wang, J.; Lu, H. Controlled Synthesis and Enzyme-Induced Hydrogelation of Poly(l-phosphotyrosine)s via Ring-Opening Polymerization of α -Amino Acid N-Carboxyanhydride. *ACS Macro Lett.* **2015**, *4*, 1000–1003.
- (18) Hu, J.; Zhang, G.; Liu, S. Enzyme-responsive polymeric assemblies, nanoparticles and hydrogels. *Chem. Soc. Rev.* **2012**, *41*, 5933–5949.
- (19) Shahriari, M.; Zahiri, M.; Abnous, K.; Taghdisi, S. M.; Ramezani, M.; Alibolandi, M. Enzyme responsive drug delivery systems in cancer treatment. *J. Controlled Release* **2019**, *308*, 172–189.
- (20) Lee, J. S.; Groothuis, T.; Cusan, C.; Mink, D.; Feijen, J. Lysosomally cleavable peptide-containing polymersomes modified with anti-EGFR antibody for systemic cancer chemotherapy. *Biomaterials* **2011**, *32*, 9144–9153.
- (21) Lotti, F.; Jarrar, A. M.; Pai, R. K.; Hitomi, M.; Lathia, J.; Mace, A.; Gantt, G. A.; Sukhdeo, K.; DeVecchio, J.; Vasanji, A.; Leahy, P.; Hjelmeland, A. B.; Kalady, M. F.; Rich, J. N. Chemotherapy activates cancer-associated fibroblasts to maintain colorectal cancer-initiating cells by IL-17A. *J. Exp. Med.* **2013**, *210*, 2851–2872.
- (22) Sun, Y.; Campisi, J.; Higano, C.; Beer, T. M.; Porter, P.; Coleman, I.; True, L.; Nelson, P. S. Treatment-induced damage to the tumor microenvironment promotes prostate cancer therapy resistance through WNT16B. *Nat. Med.* **2012**, *18*, 1359–1368.
- (23) Xu, G.; Zhang, W.; Ma, M. K.; McLeod, H. L. Human Carboxylesterase 2 Is Commonly Expressed in Tumor Tissue and Is Correlated with Activation of Irinotecan. *Clin. Cancer Res.* **2002**, *8*, 2605–2611.
- (24) Dong, H.; Pang, L.; Cong, H.; Shen, Y.; Yu, B. Application and design of esterase-responsive nanoparticles for cancer therapy. *Drug Delivery* **2019**, *26*, 416–432.
- (25) Pramod, P. S.; Shah, R.; Chaphekar, S.; Balasubramanian, N.; Jayakannan, M. Polysaccharide nano-vesicular multidrug carriers for synergistic killing of cancer cells. *Nanoscale* **2014**, *6*, 11841–11855.
- (26) Fu, J.; Qiu, L. Photo-crosslinked and esterase-sensitive polymersome for improved antitumor effect of water-soluble chemotherapeutics. *Nanomed* **2018**, *13*, 2051–2066.
- (27) Pramod, P. S.; Takamura, K.; Chaphekar, S.; Balasubramanian, N.; Jayakannan, M. Dextran Vesicular Carriers for Dual Encapsulation of Hydrophilic and Hydrophobic Molecules and Delivery into Cells. *Biomacromolecules* **2012**, *13*, 3627–3640.
- (28) Ohlsson, S. M.; Pettersson, cS.; Ohlsson, S.; Selga, D.; Bengtsson, A. A.; Segelmark, M.; Hellmark, T. Phagocytosis of apoptotic cells by macrophages in anti-neutrophil cytoplasmic antibody-associated systemic vasculitis. *Clin. Exp. Immunol.* **2012**, *170*, 47–56.
- (29) Wang, C.; Chen, S.; Wang, Y.; Liu, X.; Hu, F.; Sun, J.; Yuan, H. Lipase-Triggered Water-Responsive “Pandora’s Box” for Cancer Therapy: Toward Induced Neighboring Effect and Enhanced Drug Penetration. *Adv. Mater.* **2018**, *30*, 1706407.

- (30) Deng, Z.; Qian, Y.; Yu, Y.; Liu, G.; Hu, J.; Zhang, G.; Liu, S. Engineering Intracellular Delivery Nanocarriers and Nanoreactors from Oxidation-Responsive Polymersomes via Synchronized Bilayer Cross-Linking and Permeabilizing Inside Live Cells. *J. Am. Chem. Soc.* **2016**, *138*, 10452–10466.
- (31) Wang, X.; Liu, G.; Hu, J.; Zhang, G.; Liu, S. Concurrent Block Copolymer Polymersome Stabilization and Bilayer Permeabilization by Stimuli-Regulated “Traceless” Crosslinking. *Angew. Chem., Int. Ed.* **2014**, *53*, 3138–3142.
- (32) Hua, S.-H.; Li, Y.-Y.; Liu, Y.; Xiao, W.; Li, C.; Huang, F.-W.; Zhang, X.-Z.; Zhuo, R.-X. Self-Assembled Micelles Based on PEG-Polypeptide Hybrid Copolymers for Drug Delivery. *Macromol. Rapid Commun.* **2010**, *31*, 81–86.
- (33) Du, N.; Guo, W.; Yu, Q.; Guan, S.; Guo, L.; Shen, T.; Tang, H.; Gan, Z. Poly(d,l-lactic acid)-block-poly(N-(2-hydroxypropyl)-methacrylamide) nanoparticles for overcoming accelerated blood clearance and achieving efficient anti-tumor therapy. *Polym. Chem.* **2016**, *7*, 5719–5729.
- (34) Vyhňalkova, R.; Eisenberg, A.; van de Ven, T. Bactericidal Block Copolymer Micelles. *Macromol. Biosci.* **2011**, *11*, 639–651.
- (35) Samarajeewa, S.; Shrestha, R.; Li, Y.; Wooley, K. L. Degradability of Poly(Lactic Acid)-Containing Nanoparticles: Enzymatic Access through a Cross-Linked Shell Barrier. *J. Am. Chem. Soc.* **2012**, *134*, 1235–1242.
- (36) Qiu, N.; Gao, J.; Liu, Q.; Wang, J.; Shen, Y. Enzyme-Responsive Charge-Reversal Polymer-Mediated Effective Gene Therapy for Intraperitoneal Tumors. *Biomacromolecules* **2018**, *19*, 2308–2319.
- (37) Zhu, Y.; Yang, B.; Chen, S.; Du, J. Polymer vesicles: Mechanism, preparation, application, and responsive behavior. *Prog. Polym. Sci.* **2017**, *64*, 1–22.
- (38) Bonduelle, C. Secondary structures of synthetic polypeptide polymers. *Polym. Chem.* **2018**, *9*, 1517–1529.
- (39) Deming, T. J. Synthesis of Side-Chain Modified Polypeptides. *Chem. Rev.* **2016**, *116*, 786–808.
- (40) Qiu, N.; Liu, X.; Zhong, Y.; Zhou, Z.; Piao, Y.; Miao, L.; Zhang, Q.; Tang, J.; Huang, L.; Shen, Y. Esterase-Activated Charge-Reversal Polymer for Fibroblast-Exempt Cancer Gene Therapy. *Adv. Mater.* **2016**, *28*, 10613–10622.
- (41) Mu, J.; Lin, J.; Huang, P.; Chen, X. Development of endogenous enzyme-responsive nanomaterials for theranostics. *Chem. Soc. Rev.* **2018**, *47*, 5554–5573.